

Spatial distribution and functional significance of activated vinculin in living cells

Hui Chen,¹ Daniel M. Cohen,¹ Dilshad M. Choudhury,¹ Noriyuki Kioka,² and Susan W. Craig¹

¹Department of Biological Chemistry, Johns Hopkins University School of Medicine, Baltimore, MD 21205

²Division of Applied Life Sciences, Graduate School of Agriculture, Kyoto University, Sakyo-ku, Kyoto 606-8502, Japan

Conformational change is believed to be important to vinculin's function at sites of cell adhesion. However, nothing is known about vinculin's conformation in living cells. Using a Forster resonance energy transfer probe that reports on changes in vinculin's conformation, we find that vinculin is in the actin-binding conformation in a peripheral band of adhesive puncta in spreading cells. However, in fully spread cells with established polarity, vinculin's conformation is variable at focal adhesions. Time-lapse imaging reveals a gradient of conformational change that precedes loss of vinculin from

focal adhesions in retracting regions. At stable or protruding regions, recruitment of vinculin is not necessarily coupled to the actin-binding conformation. However, a different measure of vinculin conformation, the recruitment of vinxin β by activated vinculin, shows that auto-inhibition of endogenous vinculin is relaxed at focal adhesions. Beyond providing direct evidence that vinculin is activated at focal adhesions, this study shows that the specific functional conformation correlates with regional cellular dynamics.

Introduction

Vinculin is a 116-kD, cytoskeleton-associated protein that is essential for brain and heart development in mice (Xu et al., 1998a) and for muscle contraction in nematodes (Barstead and Waterston, 1991). Vinculin is expressed in most cell types and tissues (Otto, 1990), but its localization in muscle is particularly informative. In skeletal and cardiac muscle, vinculin describes a subsarcolemmal lattice of transmembrane connections or costameres (Craig and Pardo, 1983; Pardo et al., 1983a,b; Shear and Bloch, 1985) that attach the myofibrils to the sarcolemma (Pierobon-Bormioli, 1981) and transduce force laterally through the extracellular matrix to neighboring myocytes (Street, 1983; Ervasti, 2003). Vinculin is also enriched at myotendinous junctions (Shear and Bloch, 1985) and intercalated discs (Koteliansky and Gneushev, 1983; Pardo et al., 1983a), intercellular adhesion structures involved in longitudinal transmission of forces between adjacent muscle cells. Vinculin likely plays a role in muscle structure and stability to mechanical forces. Recent data shows that hearts of *vin*^{+/-} mice are predisposed to stress-induced cardiomyopathy (Zemljic-Harpf et al., 2004). In several cases, mutations and deletion of metavinculin,

the muscle-specific spliceform of vinculin (Byrne et al., 1992), are correlated with idiopathic dilated cardiomyopathy (Maeda et al., 1997; Olson et al., 2002), offering additional support for the importance of these proteins in muscle function.

Evidence from cells in culture suggests that vinculin functions in transducing force across cell membranes (Danowski et al., 1992; Alenghat et al., 2000), in regulating cell adhesion and motility (Rodriguez Fernandez et al., 1993; Xu et al., 1998b; DeMali et al., 2002), in controlling cell survival (Subauste et al., 2004), and in executing rac-mediated signaling events (DeMali et al., 2002; Goldmann and Ingber, 2002). In cultured cells, vinculin is enriched at cell-cell and cell-matrix junctions (Geiger, 1979) but is in equilibrium with a large cytoplasmic pool (Lee and Otto, 1997). When cells adhere and spread on ECM, a portion of the cytoplasmic vinculin is recruited to specialized sites on the plasma membrane called focal adhesions and focal contacts. At these sites, dynamic connections are made between the actin cytoskeleton and ECM through transmembrane integrin and syndecan receptors for extracellular matrix molecules. These connections relay force across the membrane (Balaban et al., 2001; Beningo et al., 2001; Galbraith et al., 2002; Tan et al., 2003) and are essential for regulation of cell motility (Palecek et al., 1997; Priddle et al., 1998). Focal adhesions appear to be compositionally, structurally, and functionally analogous to the costameres of skeletal and cardiac muscle and the dense plaques of smooth muscle cells and are

Address correspondence to Susan W. Craig: sraig@jhmi.edu

Abbreviations used in this paper: FRET, Forster resonance energy transfer; SE, sensitized YFP emission; Vh, vinculin head domain; *vin*^{-/-} MEC, vinculin null mouse embryo cells; Vt, vinculin tail domain.

The online version of this article includes supplemental material.

therefore a good model system to examine the mechanism and significance of vinculin action.

Because vinculin lacks intrinsic enzymatic activity, it must exert its functions through interaction with other proteins. Indeed, multiple proteins, including F-actin, talin, α -actinin, α -catenin, vinexin, VASP, ponsin, CAP, arp2/3 (DeMali et al., 2002), Raver-1 (Huttelmaier et al., 2001), PKC (Tigges et al., 2003), and paxillin, interact with specific domains of vinculin in vitro and colocalize with vinculin at ECM contacts in vivo (for reviews see Critchley, 2000; Zamir and Geiger, 2001). However, in contrast to isolated domains of vinculin and to vinculin immobilized on nitrocellulose, full-length vinculin in solution binds poorly or undetectably to many of these ligands (Johnson and Craig, 1994, 1995; Kroemker et al., 1994; Huttelmaier et al., 1998; Bakolitsa et al., 2004). The inert state of vinculin is caused by high affinity intramolecular binding between the vinculin head domain (Vh; residues 1–851 or 1–857) and tail domain (Vt; residues 884–1066) of vinculin (Johnson and Craig, 1994). In bimolecular assays, the K_d of the Vh–Vt complex is ~ 50 nM (Johnson and Craig, 1994); in an intramolecular context the interaction is estimated, but not directly measured, to be $< 1 \times 10^{-9}$ (Bakolitsa et al., 2004). Thus, it is implicit that disruption of the Vh–Vt interaction is required for vinculin activation and subsequent assembly of vinculin-containing protein complexes at adhesion junctions (Johnson and Craig, 1995).

Nevertheless, the model for vinculin activation and function is supported solely by in vitro biochemistry using purified proteins and their domains. Nothing is known about vinculin conformation in cells, its relevance to focal adhesion composition, or its relationship to cellular dynamics. Here, we present data providing new insights on all three of these issues.

Results

Construction of vinculin Förster resonance energy transfer (FRET) probes

To monitor activation of vinculin, we developed FRET probes using CFP and YFP as the donor-acceptor pair (Miyawaki and Tsien, 2000). Because the crystal structure of full-length vinculin was not known, we began by positioning ECFP and EYFP on the NH₂- and COOH-terminal residues of vinculin (CVY; Fig. 1 A). In cell lysates prepared from HEK 293 cells transfected with CVY, the corrected FRET emission ratio (see Materials and methods) of CVY was 0.05, only slightly greater than the baseline for CFP alone which was set to zero for the calculation. The calculated FRET efficiency (see Materials and methods) for CVY was only 3%, indicating that the NH₂ and COOH termini are not in proximity. In addition, there was little change in FRET of the CVY probe upon activation of vinculin by IpaA and binding to actin (unpublished data).

Because CVY was not a suitable FRET probe, we explored internal placements for one of the fluorescent proteins. The intramolecular distance between the NH₂ and COOH termini of Vt measured from the crystal structure of Vt (Bakolitsa et al., 1999) is ~ 14 Å. Thus, we anticipated strong FRET from

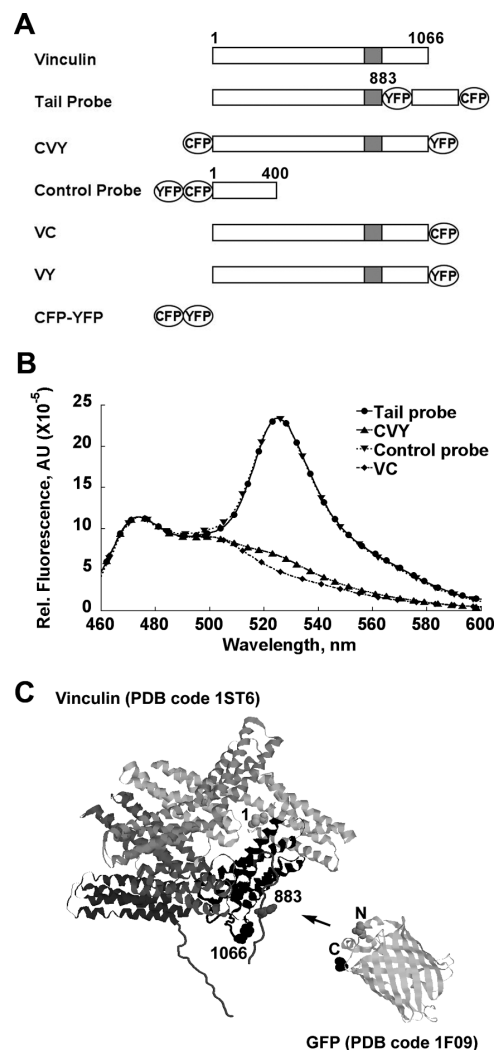


Figure 1. Structure and spectral properties of the FRET probes. (A) Schematic structure of vinculin FRET probes. (B) The emission spectra of vinculin_{1,883}-EYFP-vinculin₈₈₄₋₁₀₆₆-ECFP (Tail Probe), ECFP-vinculin-EYFP (CVY), EYFP-ECFP-vinculin_{1,400} (control probe), and vinculin-ECFP (VC). Numbers refer to amino acid residues in chicken vinculin (Coutu and Craig, 1988). Spectra were normalized to the emission of VC at 475 nm. (C) The structures of vinculin and GFP showing the size of each molecule. The arrow marks the site of YFP insertion between residues 883 and 884.

a construct in which CFP and YFP are positioned at the two ends of Vt. Indeed, an EYFP/Vt/ECFP fusion protein exhibited robust FRET (emission ratio of 1.3; efficiency of 43%) and maintained the ability to bind to Vh (unpublished data). Therefore, to construct a full-length vinculin FRET probe we inserted EYFP into vinculin at the beginning of the tail domain and placed an ECFP at the COOH terminus of vinculin to make the FRET probe, referred to as tail probe (Fig. 1, A and C).

Characterization of tail probe

Tail probe and various control constructs were expressed in HEK293 cells, and lysates were analyzed by spectrofluorimetry. Tail probe exhibited a strong FRET signal (Fig. 1 B), with a corrected emission ratio of 1.48 and an efficiency of 46% (see Fig. 4, A and B). To determine whether or not intermolecular FRET contributes to the FRET measurement, we compared a

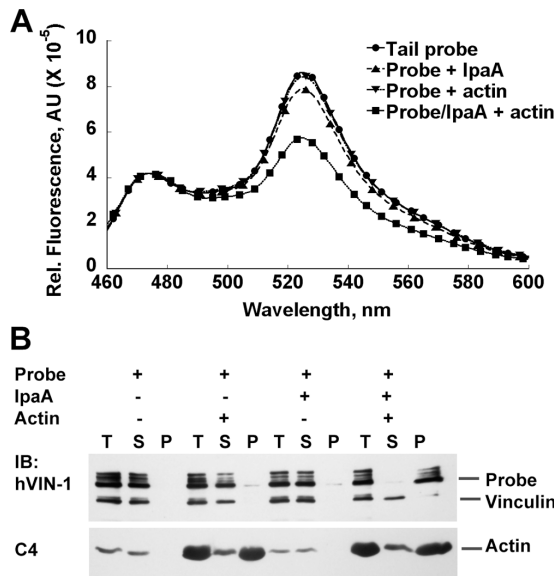


Figure 2. Response of tail probe to ligands. The binding of actin filaments to IpaA-activated vinculin tail probe induced FRET loss, indicating a conformational change of vinculin in the tail domain. (A) Normalized fluorescence emission spectra of cell lysate from HEK 293 cells transfected with tail probe in the absence or presence of 1 μ M IpaA or 5 μ M actin or both. Spectra were normalized to the emission of tail probe at 475 nm. (B) Samples from A were spun in an Airfuge (Beckman Coulter) at 25 psi (130,000 g) for 35 min. Equivalent amounts of total sample before spin (T), supernatant (S), and pellet (P) fractions were subjected to SDS-PAGE and immunoblotted with hVIN1 and C4 mAbs (Sigma-Aldrich) to vinculin and actin, respectively.

lysate containing tail probe at 5, 10, and 20 nM with mixtures of lysates containing vinculin/CFP and vinculin/YFP at 5, 10, or 20 nM each in the mixture. At all concentrations tested, the corrected FRET ratio of the mixed probes was close to that of CFP only, whereas the corrected FRET ratio of tail probe was insensitive to dilution. Thus, the FRET values obtained for tail probe report specifically on intramolecular FRET.

SDS-PAGE of HEK 293 cell lysates and Western blotting revealed that tail probe shows three closely spaced bands near the expected molecular weight. All species were recognized by both antivinculin and anti-GFP, which cross-reacted with CFP and YFP (Fig. S1, available at <http://www.jcb.org/cgi/content/full/jcb.200410100/DC1>). No evidence of proteolytic cleavage of CFP or YFP was detected in the form of GFP-sized bands. Because there is SDS-resistant structure in the CFP and/or YFP moieties (Fig. S2, available at <http://www.jcb.org/cgi/content/full/jcb.200410100/DC1>), the heterogeneity in migration of the FRET probe likely represents a combination of the fully denatured form (slowest migrating) and faster migrating, partially folded intermediates.

To determine the conformational state of tail probe and to assess its ability to report on activation of vinculin, we measured FRET response as a function of ligand binding to vinculin. Neither tail probe nor endogenous vinculin cosedimented with F-actin, indicating that the probe and endogenous vinculin were in a conformationally closed and inactive state (Fig. 2 B). As expected, addition of F-actin caused no change in the FRET signal of the probe (Figs. 2 A). To stimulate vinculin to bind F-actin, we treated lysates with IpaA. IpaA is a *Shigella flexneri*

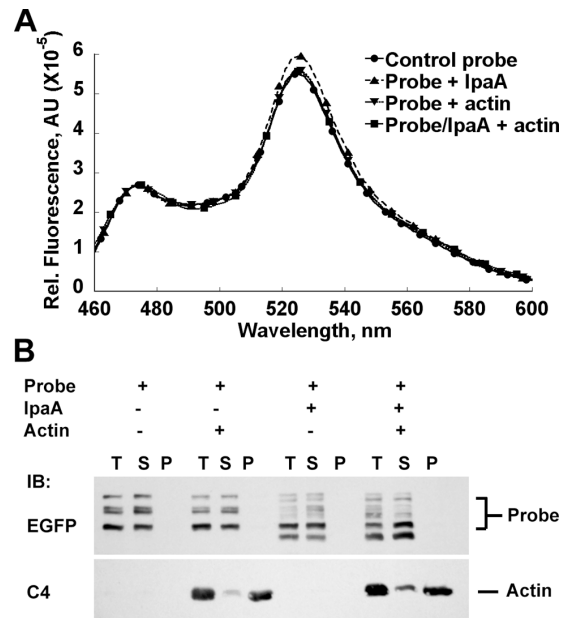


Figure 3. Response of the control FRET probe YC-V₁₋₄₀₀ to ligands. (A) Normalized fluorescence emission spectra of cell lysates from HEK 293 cells transfected with the control FRET probe in the absence or in the presence of 1 μ M IpaA or 5 μ M actin or both. Spectra were normalized to emission at 475 nm of control probe alone. The control probe preserves the IpaA binding site and a focal adhesion targeting signal of vinculin but lacks the actin binding site. It does not display FRET change in response to IpaA binding. (B) Actin cosedimentation assay, performed under the same conditions as in Fig. 2 B, showed that the control probe did not bind to actin filaments under conditions in which tail probe did bind.

virulence protein that binds to the D1 domain (residues 1–258; see Bakolitsa et al. [2004] for nomenclature reflecting new structure-based subdivisions of vinculin domains) of vinculin head and exposes the actin binding activity of vinculin tail (Bourdet-Sicard et al., 1999). Addition of IpaA alone did not cause a change in FRET, but subsequent addition of F-actin caused a 45% decrease in the corrected FRET ratio (1.48 to 0.81) of tail probe and 14% decrease in FRET efficiency (46% to 32%), reflecting a change in the conformation of vinculin (Fig. 2 A; and see Fig. 4, A and B). Tail probe cosedimented with actin filaments only in the presence of IpaA, demonstrating that the loss of FRET reports on binding of IpaA-activated tail probe to F-actin (Fig. 2 B).

Tail probe and endogenous vinculin differ in their sensitivity to IpaA (Fig. 2 B). This difference is abolished by inclusion of 1% Triton X-100 in the lysate (unpublished data). The requirement of Triton X-100 for IpaA activation of endogenous vinculin in cell lysates is unexpected because IpaA can activate at least 40% of purified smooth muscle vinculin and recombinant vinculin in vitro without the presence of Triton X-100 (Bourdet-Sicard et al., 1999; see Fig. 9). The differential response between the tail probe and endogenous vinculin reflects a more tightly closed conformation in endogenous vinculin, which may be mediated by a Triton X-100-sensitive component in the lysate. Despite this difference, the inability of the tail probe to cosediment with actin filaments shows that like endogenous vinculin, it adopts an autoinhibited conformation. Furthermore, tail probe and vinculin localize similarly in cells

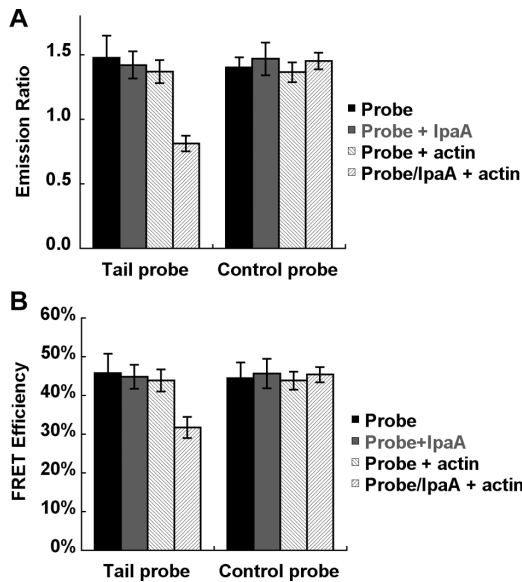


Figure 4. **Corrected emission ratios and FRET efficiencies of vinculin FRET probes.** The mean emission ratios corrected for spectral cross talk (A), and the extracted FRET efficiencies (B) were obtained as described in Materials and methods. $n = 3$. Error bars are the SEM.

and are equally able to rescue spreading defects in vinculin null cells (see Fig. 5).

For a control probe, we constructed an EYFP-ECFP chimera fused in frame to vinculin residues 1–400 (Fig. 1 A). This probe contains the binding site for IpaA (Bourdet-Sicard et al., 1999) and a focal adhesion targeting motif (Bendori et al., 1989) but lacks F-actin binding capacity (Menkel et al., 1994). Control probe had a corrected FRET ratio of 1.4 and a FRET efficiency of 44% (see Fig. 4, A and B). These values are similar, fortuitously, to unstimulated tail probe in cell lysates. This property was useful because it allowed us to use the FRET signal of control probe observed in cells to define the baseline FRET for the closed conformation of tail probe. There was no significant change in FRET for the control probe in cell lysates either before or after treatment with IpaA, actin, or both ligands together (Fig. 3 A; and Fig. 4, A and B); nor did the control probe cosediment with actin (Fig. 3 B). Therefore, we conclude that tail probe reports on conformational changes in vinculin that reflect its activation and binding to actin filaments, whereas control probe is insensitive to F-actin and to IpaA, an activator of the Vh.

When transfected into vinculin null mouse embryo cells ($vin^{-/-}$ MEC; Xu et al., 1998a), both the tail probe and untagged vinculin showed a diffuse cytoplasmic pool and were similarly enriched at focal adhesions (Fig. 5 A). Tail probe and untagged vinculin were equally able to rescue the spreading defect (Xu et al., 1998a,b) and change in cell shape (DeMali et al., 2002) as shown in Fig. 5 (C and E and B and D, respectively). Thus, the vinculin tail FRET probe is suitable for analysis of vinculin conformation in living cells.

Detection of tail probe FRET in living cells

To determine if vinculin conformation correlates with subcellular localization, we transfected $vin^{-/-}$ MEC with tail probe and

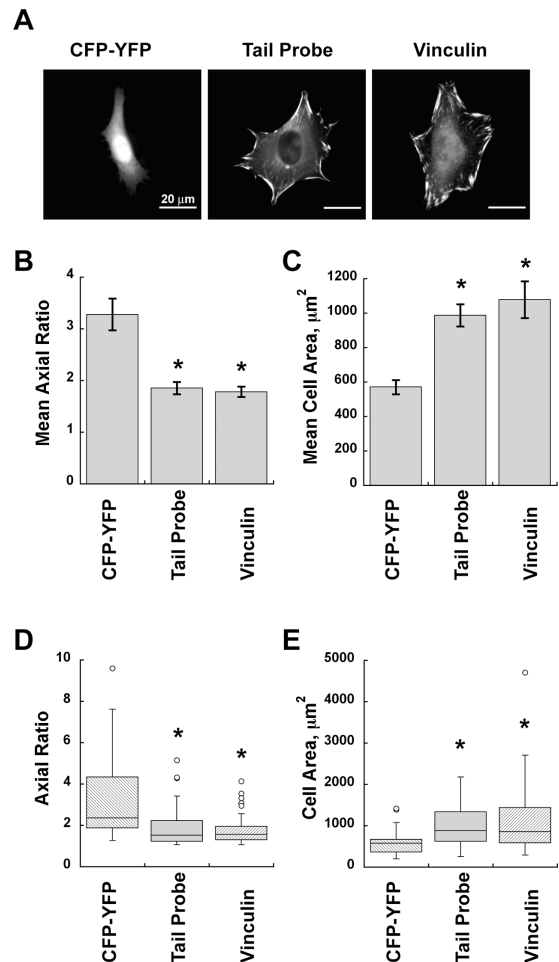


Figure 5. **Vinculin tail probe rescues spreading and lamellipodial extension on fibronectin.** (A) Vinculin null cells expressing a control CFP-YFP chimera, tail probe, or untagged vinculin were allowed to spread onto 20 μg/ml of FN for 2 h at 37°C. Cells expressing untagged vinculin were stained with Vin11-5 antibody and rhodamine-conjugated secondary antibody. Cells expressing CFP-YFP and tail probe were examined by GFP fluorescence. (B–D) The extent of spreading was quantified by measuring the ratio of major/minor axis of cells (B and D) and cell areas (C and E). (B and C) Mean of the axial ratio and cell area, respectively. Error bars are the SEM. (D and E) Box plots (Chase and Brown, 1997) of B and C. Each box encloses 50% of the data with median value displayed as a horizontal line. Top and bottom of box represent the limits of $\pm 25\%$ of the population. Lines extending from top and bottom of boxes mark the minimum and maximum values of the data set that fall within an acceptable range. Open circles denote outliers, points whose value is either $>UQ + 1.5 \times IQD$ or $<LQ - 1.5 \times IQD$ (UQ, upper quartile; IQD, inter-quartile distance; LQ, lower quartile). Asterisks mark histograms that are statistically different from the corresponding control. The tail probe ($n = 56$) or untagged vinculin ($n = 49$) reexpressing cells are significantly ($P < 0.01$) more spread than $vin^{-/-}$ cells ($n = 44$).

calculated a FRET image from the digital data as described in Materials and methods. The global emission ratio (averaged over all pixels above threshold) observed in these cells was 1.43 ± 0.18 SD ($n = 8$, compiled from two experiments), which was distinguishable from the baseline of 0.6 obtained from cells transfected with vinculin/CFP. To confirm that the emission ratio reflects FRET, the average FRET efficiency of tail probe in cells was determined by fluorescence recovery after acceptor photobleaching and found to be $\sim 15\%$ (Fig. S3, available at <http://www.jcb.org/cgi/content/full/jcb.200410100/DC1>).

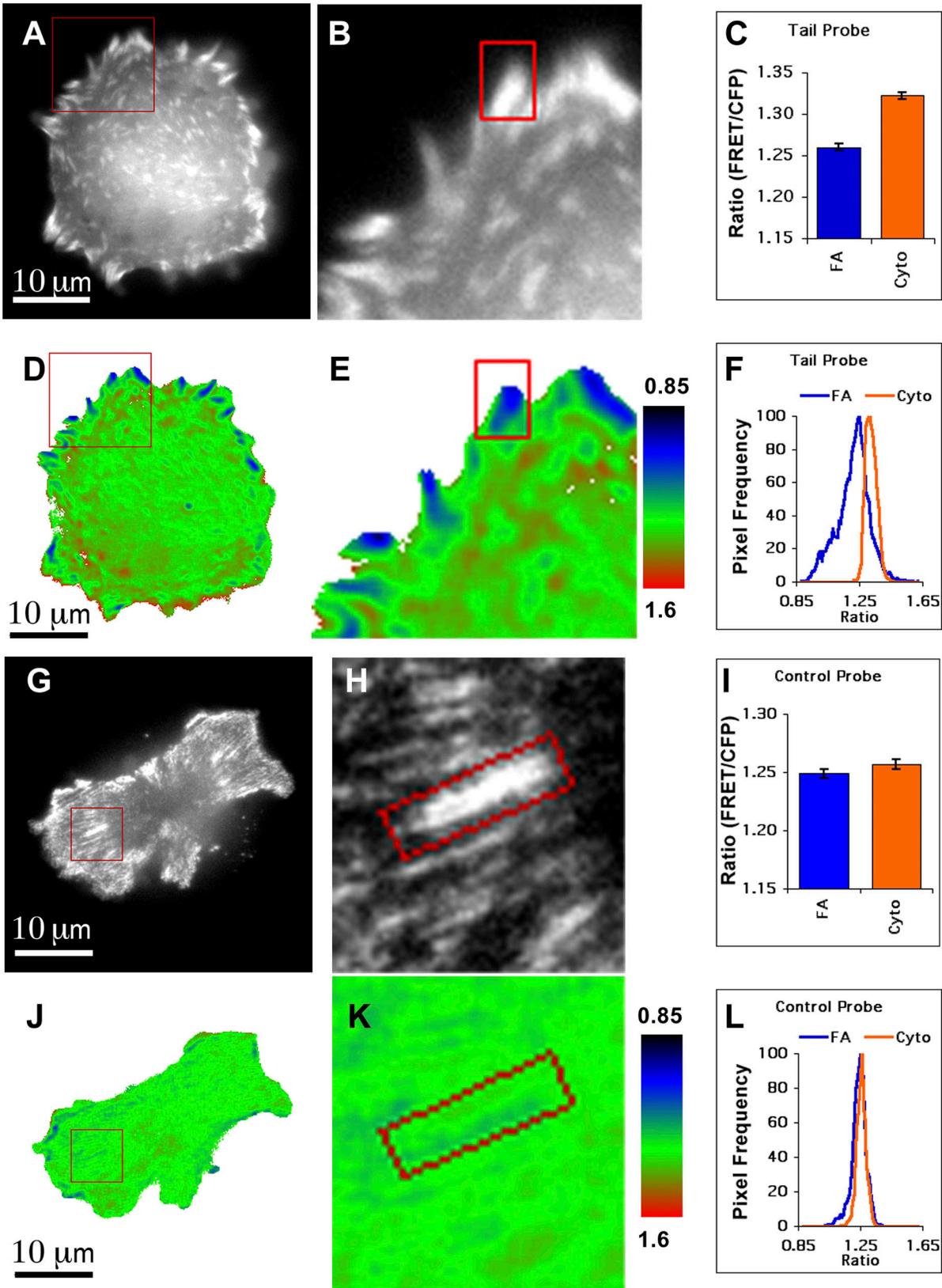


Figure 6. **Spatial distribution of activated vinculin in living cells.** *Vin*^{-/-} MEC transfected with tail probe (A–F) or control probe (G–L) were imaged 1 h after plating. (A and G) Localization of tail probe and control probe in MECs imaged through CFP channel. (D and J) Pseudocolored ratio (FRET/CFP) image of the cells shown in A and G. (B, E, H, and K) Enlargement of boxed region in A, D, G, and J, respectively. (C and I) The average FRET ratio measured from segmented regions of cytoplasm or focal adhesions; all segmentable focal adhesions were included. (F and L) Histograms of FRET ratios measured from the segmented focal adhesions and cytoplasm. Notably, the tail probe gave a much lower average FRET ratio (corresponding to actin-binding conformation of vinculin) in focal adhesions (B and E, boxed region) than in cytoplasm even though not all focal adhesions are distinguishable from cytoplasm. The control probe did not distinguish between the two locations (H and K, boxed region). Similar results were obtained by analysis of three other cells from a separate experiment.

Spatial resolution of vinculin conformations in living cells

When focal adhesions were examined in *vin*^{-/-} MEC transfected with tail probe, we found that the average FRET ratio is significantly lower in focal adhesions than in cytoplasm (Fig. 6, A–F), indicating enrichment of the actin-binding conformation in focal adhesions. In contrast, in *vin*^{-/-} MEC transfected with the control probe (YC/V 1–400), the FRET ratio is similar in focal adhesions and in cytoplasm (Fig. 6, G–L). The FRET ratio of tail probe in cytoplasm is comparable to the global FRET ratio of control probe (Fig. 6, D, F, J, and L), indicating that vinculin is in the nonactin binding conformation in the cytoplasm. Although the actin-binding conformation of vinculin is enriched in focal adhesions, there were regions of the cell in which the conformation of vinculin in the focal adhesions was not readily distinguished from that in cytoplasm (Fig. 6, com-

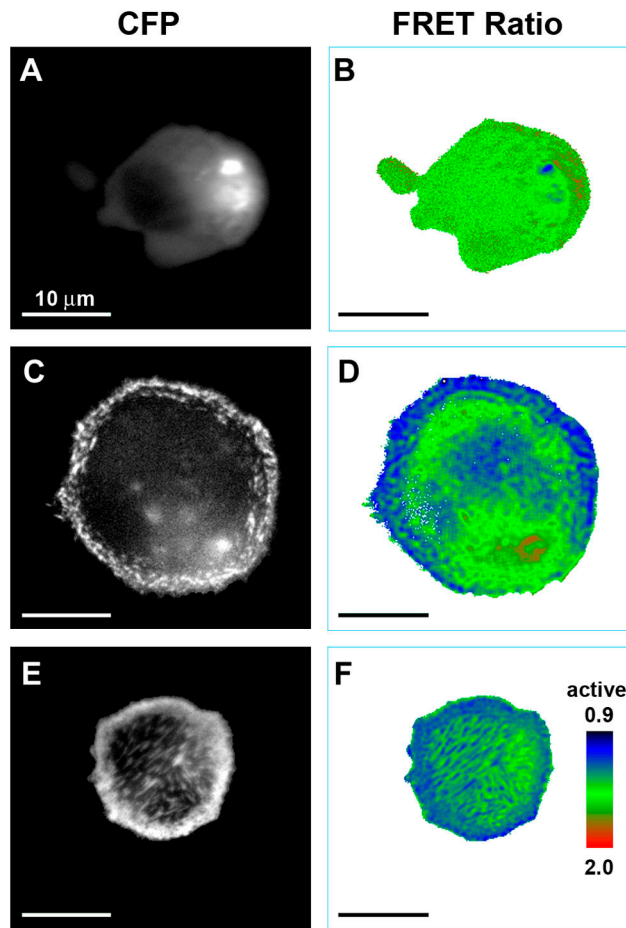


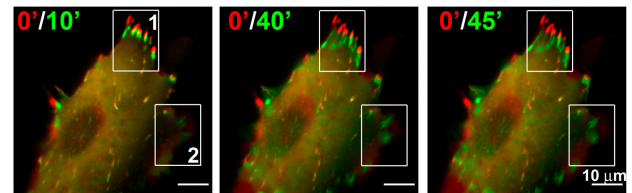
Figure 7. Recruitment of vinculin to the peripheral belt of adhesion puncta during cell spreading is associated with conformational activation of vinculin. *Vin*^{-/-} MECs transfected with tail probe were replated into a dish (Bioptechs) coated with 20 μ g/ml fibronectin heated at 37°C. (A and B) Images of a representative cell at the initial attachment stage \sim 5 min after plating. (C–F) Images of two representative cells at \sim 45–60 min after plating. (A, C, and E) Localization of tail probe in each *Vin*^{-/-} MEC imaged through CFP channel. (B, D, and F) Pseudocolored ratio (FRET/CFP) image of the cells shown in A, C, and E. Notably, the adherent rounded cell (A and B) gave a high FRET ratio, similar to that of cells containing control probe (Fig. 6), indicating that vinculin was largely closed in conformation at the earliest stages of spreading. During spreading, tail probe showed lower FRET ratios correlating with actin-binding conformation in adhesion structures (C–F).

pare A with D). Similar results were obtained from analysis of three other cells in separate experiments.

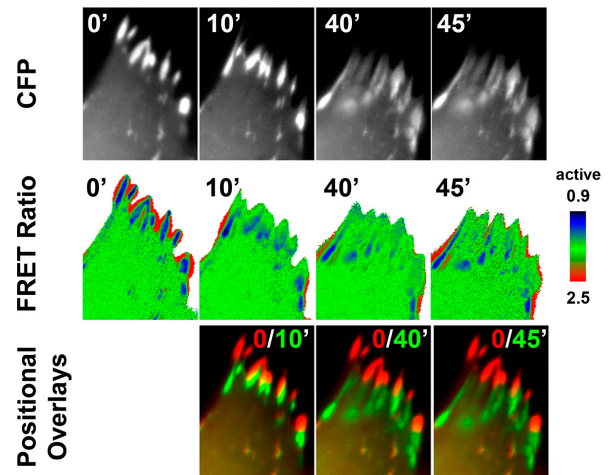
Correlation of vinculin conformation with cellular dynamics

To explore the heterogeneity of vinculin conformation in focal adhesions, we asked whether or not the average conformation

A. Dynamics of Vinculin in Focal Adhesions



B. Zoom of Panel A, Region 1



C. Zoom of Panel A, Region 2

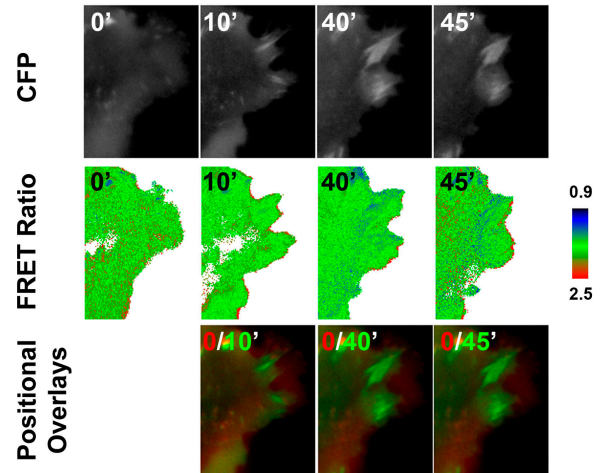


Figure 8. The conformation of vinculin during focal adhesion dynamics. 24 h after plating, a fully spread smooth muscle cell was imaged at time 0, 10, 40, and 45 min. Images were corrected for photobleaching before calculation of the FRET ratio image. (A) The positions of the cell at later time points (green) relative to 0 time point (red) were displayed as color joins of CFP images. (B) Enlargement of the retraction zone from region 1 in A. Notably, as mature focal adhesions disassemble, vinculin loses the actin-bound conformation in a gradient from the tip to the base of the focal adhesions. (C) Enlargement of the focal adhesion assembly zone from region 2 in A. As focal adhesions mature, recruited vinculin does not always adopt the actin-bound conformation.

correlated with cellular activity. In *vin*^{-/-} MECs that have attached to fibronectin but have not initiated spreading, vinculin is uniformly in the nonactin binding conformation (Fig. 7, A and B). At early phases of isotropic spreading, vinculin is recruited to puncta in the peripheral adhesion ring and to short central adhesions where it is largely in the actin-binding conformation (Fig. 7, C–F). Some cells (Fig. 7, C and D) showed the nonactin binding conformation of vinculin in a segment of the adhesion belt puncta (see bottom edge of cell in Fig. 7, C and D). Unfortunately, phototoxicity associated with acquiring the FRET image precluded correlating these asymmetric regions with subsequent events in cell spreading.

Fully spread smooth muscle cells were more photoresistant, enabling limited time-lapse analysis in cells that had spread for 24 h and were undergoing localized, asymmetric cell shape changes. We found that in retracting/contracting regions of the cell there is loss of the actin-binding conformation before loss of vinculin from focal adhesions (Fig. 8, A and B, region 1, compare 0- and 10-min time points). Interestingly, a gradient of vinculin conformation can be observed in which the

actin binding conformation is found at the proximal edge of the gliding or disassembling focal adhesion even out to 45 min.

In contrast, a different region of the same cell shown in Fig. 8 showed recruitment of vinculin to growing focal adhesions (Fig. 8, A and C, region 2). The recruited vinculin was not in the actin-binding conformation at the times observed. This result indicates an additional basis for the heterogeneity of the vinculin FRET ratio in fully spread MECs and also indicates that vinculin recruitment and conformational activation are separate processes.

Activation of vinculin is required for assembly of vinculin–vinexin β complexes in focal adhesions

The images of the FRET probe in living cells indicate that vinculin can exist in a conformationally open state in focal adhesions. To confirm that the FRET probe reports faithfully on the conformation of native, endogenous vinculin at focal adhesions, we took advantage of our finding that vinexin β fails to target to focal adhesions in vinculin null cells (Fig. S4, available at <http://>

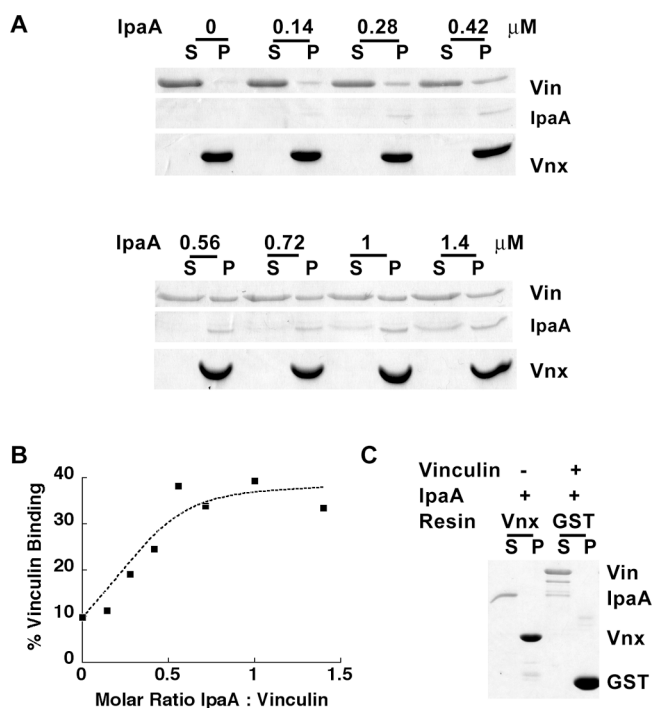


Figure 9. Vinculin binding to SH3 domains of vinexin β is conformationally regulated. (A) Vinculin, at a 1- μ M concentration, was incubated in 20 mM Pipes, pH 6.9, 100 mM KCl, and 0.1% Triton X-100 with GST-vinexin (residues 42–115, encoding the first two SH3 domains of vinexin) immobilized on glutathione-agarose beads in the presence of varying amounts of IpaA. After an overnight incubation at 4°C, supernatant (S) and pellet (P) were fractionated by centrifugation for 2 min at 10,000 g. The resin was washed twice with binding buffer before elution in Laemmli sample buffer. Equal loading of pellets and supernatants represent 10% of total reaction. Samples were analyzed by SDS-PAGE and Coomassie staining. (B) Densitometry-based quantification of vinculin–vinexin interaction based on digitized Coomassie blue–stained gel analyzed in NIH Image. (C) Coomassie-stained gel of negative controls for binding experiment shown in A. IpaA was incubated with GST-vinexin in the absence of vinculin, demonstrating that no direct interaction occurs. Furthermore, the vinculin–IpaA complex does not co-sediment with GST alone, demonstrating the specificity of the ternary complex with vinexin.

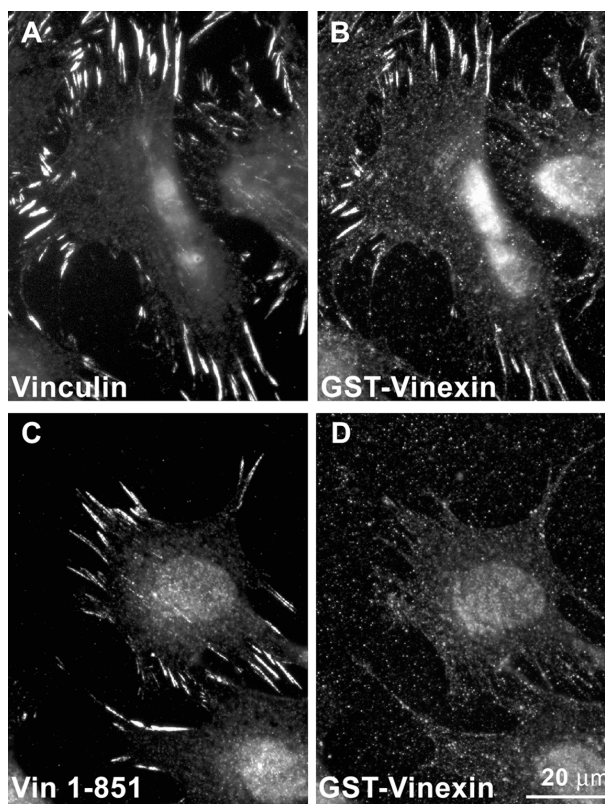


Figure 10. Vinculin mediates vinexin β recruitment to focal adhesions. Vinculin null cells were permeabilized with 0.05% digitonin and incubated with 10 μ g/mL GST-vinexin β (residues 1–329, encoding full-length vinexin) and 25 μ g/mL vinculin (A and B) or Vh (C and D) in 25 mM MES, pH 6.0, 3 mM MgCl₂, and 1 mM EGTA. Vinculin localization was visualized by staining with 5 μ g/mL of 3.24 monoclonal antivinculin, followed by Rhodamine red-X–conjugated donkey anti–mouse IgG (A and C). Vinexin was visualized by staining with 5 μ g/mL of polyclonal anti-GST followed by Oregon green–conjugated donkey anti–rabbit IgG (B and D). In the presence of full-length vinculin, vinexin β becomes strongly enriched in focal adhesions. However, vinexin β fails to target to focal adhesions in the presence of Vh, which lacks the polyproline region required for a direct interaction with vinexin.

www.jcb.org/cgi/content/full/jcb.200410100/DC1). Vinexin β uses its first and second SH3 domains to bind to the proline-rich region of vinculin (Kioka et al., 1999). However, we found that, in vitro, full-length vinculin binds poorly to the SH3(1–2) of vinexin β . Upon addition of IpaA, the amount of vinculin bound to vinexin increased linearly until binding of IpaA to vinculin reached saturation at $\sim 40\%$ of the vinculin (Fig. 9, A and B). Thus, the activated conformation of vinculin is required to bind vinexin β . We then used this property to confirm the presence of the activated conformation of vinculin in focal adhesions and to establish its functional relevance.

Using a permeabilized cell model prepared from *vin*^{-/-} MEC, we found that recruitment of exogenous vinexin β to focal adhesions was dependent on the presence of vinculin in the focal adhesions (Fig. 10, A and B). Consistent with a direct interaction between the two proteins, recruitment of vinexin β to focal adhesions depends on the presence of the vinexin binding site because Vh1-851, which lacks the site (Kioka et al., 1999), was unable to recruit vinexin (Fig. 10, C and D). Because vinculin must be activated to bind vinexin β (Fig. 9, A and B), we conclude that some of the endogenous vinculin at the focal adhesions must be in the open or activated conformation and that one functional consequence of this activated conformation is assembly of vinculin–vinexin β complexes at focal adhesions.

Discussion

Development of FRET probes for vinculin conformation illustrates the value of modular protein structure

FRET efficiency (E) declines rapidly as the inverse of the sixth power of the distance between the chromophores (r) according to the relationship $E = 1 / (1 + (r^6/R_0^6))$, in which R_0 is the calculated Forster distance for a particular donor and acceptor chromophore pair (Clegg, 1992). Therefore, to construct a FRET probe with a high FRET efficiency, the chromophores of CFP and YFP need to be positioned within $2R_0$ of each other, where R_0 is the distance between donor and acceptor at which the FRET efficiency is 50%. The calculated R_0 for the CFP/YFP pair is 49 Å (Patterson and Piston, 2000), assuming random orientation between donor emission and acceptor absorbance dipoles.

Initially we placed the donor and acceptor GFP variants at NH₂ and COOH termini of vinculin to monitor the conformation of the whole molecule. This construct (CVY) gave a barely detectable FRET signal due to long distance or unfavorable angle (or both) between donor and acceptor chromophores. The GFP proteins are β barrels with dimensions of $\sim 40 \times 30$ Å and the chromophore sits in the middle of the barrel that has a radius of ~ 15 Å (Ormo et al., 1996; Yang et al., 1996). In a FRET pair dimer, the two chromophores are separated by ~ 30 Å, reducing maximum FRET efficiency to 95%. Based on recent crystal structures of intact vinculin (Bakolitsa et al., 2004; Borgon et al., 2004) and vinculin domains (Izard et al., 2004), there is ~ 40 Å from the amino- to carboxy-terminal end of vinculin. The very low FRET of the CVY construct is consistent with the possibility that as much as 70 Å could sepa-

rate the chromophore centers. Thus, the FRET of CVY indicates that the crystal structure is a good representation of the inactive conformation of vinculin in solution phase.

Because vinculin is a modular protein (Coutu and Craig, 1988; Price et al., 1989), it offered the possibility that self-folding, single-domain proteins such as the GFP variants could be inserted between modules of the protein, as was done for fibronectin (Ohashi et al., 1999). The success of this approach is facilitated by the fact that the NH₂- and COOH-terminal ends of GFP are close to each other and contain short unstructured regions that can serve as linker sequences (Fig. 1 C). Our data show that it is possible for GFP modules to be inserted in the loop between two functional domains of a protein, with appropriate spacers, without interfering significantly with the functions of the molecule. Such probes should be especially useful for monitoring signal-induced functional changes in molecules that lack enzymatic activity, such as the structural cytoskeletal proteins and extracellular matrix molecules. With appropriately characterized probes it may be possible to study directly how cellular mechanical activity affects the structure and function of the ECM and cytoskeletal proteins in living cells, and indeed some pioneering work in this vein has been done (Ohashi et al., 1999).

The conformation of vinculin in cytoplasm versus focal adhesions: validation of the recruitment and activation hypothesis

Vinculin is proposed to modulate the junction between ECM and the actin cytoskeleton by linking an integrin and talin complex to the actin network (Horwitz et al., 1986). Because biochemical data show that vinculin can bind neither talin nor actin unless the intramolecular interaction between head and tail is released, the prediction is that vinculin at focal adhesions must adopt an active conformation. Our live cell data shows a striking concentration of the actin-binding conformation of vinculin in focal adhesions as compared with cytoplasm, supporting the central prediction of the aforementioned model for vinculin recruitment and activation. For cytoplasmic vinculin, the FRET data allows us to conclude that the conformation of cytoplasmic vinculin is inactive, at least with respect to its actin-binding potential.

The conformation of vinculin in focal adhesions: new insights

Detailed inspection of the cellular FRET data show that the aforementioned model of recruitment and activation of vinculin at focal adhesions is oversimplified. Specifically, in some cells, there was polarity in distribution of the actin-binding conformation of vinculin at focal adhesions. To explore this heterogeneity we asked whether the average conformation of vinculin in an adhesive structure correlated with membrane dynamics. Although our ability to do sequential FRET captures on a cell is limited by phototoxicity and photolability issues, we were able to do limited time-lapse sequences on smooth muscle cells transfected with tail probe. These images revealed that the heterogeneity of vinculin conformation in focal adhesions correlated with regional cell dynamics in fully spread

cells undergoing localized changes in cell shape. Peripheral focal adhesions were enriched for the actin-binding conformation of vinculin, but showed a loss of that conformation upon membrane retraction and focal adhesion disassembly. Interestingly, there was a gradient of vinculin conformation that proceeded from the distal tip toward the proximal edge of the focal adhesions, with the proximal edge being the last to show the nonactin binding conformation. Thus, one source of the heterogeneity of vinculin conformation in focal adhesions is related to regional retraction of the plasma membrane.

When observing retraction events in a cell it is important to consider whether one is simply observing global retraction induced by phototoxicity. Thus, we analyzed only cells that had regions that were stable or protruding at the same time that another region was retracting. This analysis resulted in finding another source of heterogeneity in vinculin conformation. In stable regions of the cell membrane in which vinculin was being recruited to focal adhesions, the vinculin remained in the nonactin binding conformation. Thus recruitment is not necessarily synonymous with actin binding and a second signal or event must be required to link vinculin to actin.

In previous work, it has been observed that recruitment of vinculin is correlated with adhesive strengthening (Galbraith et al., 2002) and with localized application of tension to cell membrane (Balaban et al., 2001), implying vinculin-mediated strengthening of connections to the cytoskeleton. Because recruitment of vinculin to focal adhesions and binding of vinculin to actin are not always coupled events, one can envision that modulating the actin-binding conformation of vinculin may be a cellular response to changes in the amount of tension experienced by a focal adhesion.

Although we were not able to adequately determine FRET in the tiny, very dim focal complexes at the leading edge of lamellipodia, we were able to analyze vinculin conformation in spreading cells. Before initiation of spreading, vinculin is uniformly in the nonactin-binding conformation. But at early stages of spreading, when a band of vinculin-containing puncta circumscribes the edge of the spreading cell, vinculin in the puncta is largely in the actin-binding conformation. To the extent that this spreading edge mimics an advancing lamellipodium, the result suggests that vinculin in focal complexes at the leading edge would be in the actin-binding conformation, as predicted from the work of DeMali et al. (2002).

The significance of vinculin conformation at focal adhesions

We have presented biochemical and cellular evidence that conformational change of vinculin at focal adhesions is functionally correlated with ligand binding. Not only does localization of vinexin β to focal adhesions require vinculin but this recruitment results from selective binding of vinexin β to the conformationally open state of vinculin. These data provide direct evidence that the conformation of vinculin regulates focal adhesion plaque composition by direct protein–protein interactions. Moreover, in establishing that endogenous vinculin also exists in a distinct ligand-binding conformation in focal adhesions, these data confirm that the vinculin FRET probe reports faithfully on sites of vinculin activation in living cells.

Although the physiological function of the vinculin–vinexin β complex is unknown, it is interesting that ectopic expression of vinexin β stimulates cell spreading in C2C12 cells (Kioka et al., 1999), as does reexpression of vinculin in *vin*^{-/-} cells (Xu et al., 1998b). Given the requirement for activated vinculin to localize vinexin β to adhesion sites, it is intriguing to speculate that integrin-stimulated recruitment and formation of the vinculin–vinexin β complex at focal adhesions may be part of the machinery that links growth factor–stimulated processes to cell adhesion.

In summary, the vinculin FRET probe and the vinexin recruitment experiment have enabled us to demonstrate that vinculin becomes activated when it gets recruited to plasma membrane and that activation is required for particular protein–protein interactions at the focal adhesion. These results establish the relevance of the *in vitro* biochemical insights to actual cellular events. In addition, the FRET analysis reveals that, *in vivo*, conformational regulation of vinculin is more complex than the original model (Johnson and Craig, 1995). Specifically, vinculin's conformation varies amongst focal adhesions in a way that correlates with regional membrane dynamics. This result adds another layer to the heterogeneity of focal adhesions; not only do they vary in the amounts and spatial distribution of components (Zamir et al., 1999) but also in the functional conformation of the vinculin that they contain.

Materials and methods

Reagents and proteins

Actin was extracted from chicken skeletal muscle acetone powder, processed through one cycle of polymerization and depolymerization, and gel filtered through a Sephadex G-150 column according to Pardee and Spudich (1982). Recombinant 6 \times -His-tagged chicken vinculin was purified. GST–vinexin β was expressed in bacteria and purified on glutathione agarose (Smith and Johnson, 1988). pCXN2 encoding murine vinculin was provided by E. Adamson (Burnham Institute, La Jolla, CA). Details on cloning, expression, and purification of IpaA can be found in the online supplemental material.

Construction of FRET probes

To generate vinculin tail probe, first a 9-bp fragment encoding a NotI site was introduced by mutagenesis into pEGFP-C1/vinculin cDNA (chicken) immediately after the codon for aa 883 (Coutu and Craig, 1988) using the Quick Change kit (Stratagene). The cDNA of EYFP (CLONTECH Laboratories, Inc.) minus the stop codon and flanked by NotI was inserted into NotI-digested vinculin. pECFP-N3 vector was constructed as an intermediate vector for generating tail probe. ECFP was PCR amplified with 5'-GGT-ACCAtggtgagcaagggc-3' and 5'-GCGGCCGCTtactgtacagctc-3' to generate 5' KpnI and 3' NotI. The product was subcloned into TOPO pCRII and sequenced. The KpnI and NotI fragment of pCRII/ECFP was used to replace the EGFP fragment of pEGFP-N3 to generate pECFP-N3. Finally, the EcoRI–Sall fragment containing vinculin₁₋₈₈₃-YFP–vinculin₈₈₄₋₁₀₆₆ was subcloned into pECFP-N3 to generate tail probe [p ECFP-N3/V₁₋₈₈₃ GGR-YFP-GGR-V₈₈₄₋₁₀₆₆-VDGT].

To make the control FRET probe pEYFP-C1/CFPV₁₋₄₀₀, a HindIII site was engineered before the ATG site of pET15b/CFP-V₁₋₈₅₁ and a KpnI site after codon 400 by PCR amplification with 5'-CAAGCTTCGatggtgagcaagggc-3' and 5'-GGTACCTCAtgcaacttctctgc-3'. The PCR product was introduced into TOPO pCRII and sequenced. The HindIII–KpnI fragment of CFP–vinculin₁₋₄₀₀ was subcloned into pEYFP-C1 to generate the control plasmid pEYFP-CFPV₁₋₄₀₀.

Cell culture and transfection

Cells were cultured on 0.1% gelatin-coated tissue culture plates in DME with high glucose and glutamine (MediaTech) supplemented with 10% FCS in a 5% CO₂ incubator at 37°C. For cell imaging and FRET analysis, *vin*^{-/-} MECs, isolated from embryo #54^{-/-}, were cultured with home-

made phenol red-free DME (same as aforementioned DME except phenol red-free, 4750 mg/l NaCl, 370 mg/l NaHCO₃, 5958 mg/l Hepes, and one-fourth the concentration of vitamins). These media modifications reduced background and autofluorescence. HEK 293 cells were seeded on 0.1% gelatin-coated 100-mm dishes at 3 million per plate; transfection was performed the next day with 3 μg of plasmid DNA using LipofectAMINE/Plus reagent (Invitrogen). HEK 293 cells were lysed 2 d after transfection. Vin^{-/-}MECs were seeded on 20 μg/ml of fibronectin-coated 35-mm tissue culture dish at 120,000 cells; transfection was performed the next day with 1 to ~1.5 μg of plasmid DNA using LipofectAMINE/Plus reagent.

Cell spreading assay

Vin^{-/-}MEFs were transfected with tail probe, vinculin, or CFP-YFP chimera. 24 h after transfection, ~400,000 cells were seeded on coverslips coated with polylysine and 20 μg/ml of human fibronectin and incubated in 10% FCS/90% DME (MediaTech) at 37°C for 2 h. Cells transfected with tail probe and CFP-YFP chimera were fixed in 4% PFA in PBS for 20 min, washed twice with PBS, and mounted on a slide with Prolong Gold antifade reagent (Molecular Probes). For cells transfected with untagged vinculin, coverslips were fixed and immunostained with Vin11-5 (Sigma-Aldrich) and rhodamine-conjugated donkey anti-mouse IgG (Jackson ImmunoResearch Laboratories). Axial ratios and cell areas of transfected cells were measured using the segmentation and quantitation tools in IPlab (Scanalytics). Multinucleated cells were excluded from the analysis.

FRET assay of cell lysates

HEK 293 cells were detached with 1 mM EDTA in calcium- and magnesium-free PBS at 37°C for 20 min. The pelleted cells were resuspended in ice-cold hypotonic buffer (20 mM Tris, pH 7.5, 2 mM MgCl₂, 0.2 mM EGTA, 0.5 mM ATP, 0.5 mM DTT, and 2× protease inhibitor cocktails I and II [Siliciano and Craig, 1986]) at a density of 2 to ~4 × 10⁶ cells/ml, incubated on ice for 20 min, and homogenized manually for 5 min in a DUALL 21 conical ground glass homogenizer (Kontes Glass Co.). The lysate was cleared by centrifugation at 4°C, 16,000 g for 10 min. The hypotonic lysate was supplemented with KCl to a final concentration of 100 mM for fluorimetric and actin sedimentation assays. The emission spectrum of fluorescent proteins in the lysate was acquired with a Fluoromax-3 spectrofluorimeter (Jobin Yvon). CFP emission was traced from 460 to 600 nm with excitation at 440 nm, and YFP emission was traced from 510 to 600 nm with excitation at 490 nm. The increment was 1 nm and integration was 0.2 s. The excitation and emission slit widths were 3 and 5 nm, respectively. Lysate from an equal number of untransfected HEK293 cells was used to obtain a background emission spectrum. After subtraction of background, the spectra comprising a single experiment were normalized to the CFP emission of a reference spectrum, as specified in the figure legends.

Determination of the corrected FRET emission ratio and FRET efficiencies

To obtain a number for the corrected FRET emission ratio (a value related to FRET efficiency by Eq. 5) and an estimate of the FRET efficiency itself (as reported in Fig. 4), the sensitized YFP emission (SE) due to FRET was extracted from the raw FRET signal. The raw FRET signal is the EYFP emission (peak at 525) stimulated by excitation of ECFP at 440 nm. It consists of the SE, the emission from direct excitation of EYFP by 440 nm, and the overlap of the ECFP emission spectrum with the EYFP emission spectrum (Erickson et al., 2001). The latter two components of the raw FRET signal are referred to as "spectral cross talk."

To determine the amount of spectral cross talk contributed by direct excitation of EYFP by excitation at 440 nm, the value R_Y was determined from a sample containing just EYFP by the ratios of the emissions at 525 nm after excitation at 440 and 490 nm. R_Y was 0.11 in this study. The EYFP emission at 525 nm of the FRET probe after excitation at 490 nm was then multiplied by R_Y to obtain the YFP cross talk component. The YFP cross talk at 525 nm was subtracted from the raw FRET emission at 525 nm to correct for direct excitation of EYFP in the FRET probe by 440-nm excitation.

To determine the contribution of CFP emission to the signal at 525 nm after excitation of the FRET probe at 440 nm, the value R_C was determined from a sample containing just ECFP by ratioing the emission at 525 nm to that at 475 nm after excitation at 440 nm. R_C was 0.43 in this study. The corrected FRET emission ratio [ER in Eqs. 4 and 5] is the emission at 525 nm/emission at 475 nm, after correcting for the EYFP and ECFP cross talk. Corrected FRET emission ratio is SE/F_{DA}. Corrected FRET emission ratio correlates with FRET efficiency; the higher the corrected FRET emission ratio, the stronger the FRET. The expression for FRET effi-

ciency (E%), E% = (F_D - F_{DA})/F_D (Miyawaki and Tsien, 2000), is transformed to Eqs. 1–5 to express FRET efficiency in terms of SE, F_{DA}, and the quantum efficiencies of EYFP and ECFP, which are the experimentally determined parameters.

$$E\% = \frac{nF}{nF + F_{DA}} \quad (1)$$

$$= \frac{SE \times (Q_C/Q_Y)}{SE \times (Q_C/Q_Y) + F_{DA}} \quad (2)$$

$$= \frac{(SE/F_{DA}) \times (Q_C/Q_Y)}{(SE/F_{DA}) \times (Q_C/Q_Y) + 1} \quad (3)$$

$$= \frac{ER \times (Q_C/Q_Y)}{ER \times (Q_C/Q_Y) + 1} \quad (4)$$

$$E\% = \frac{ER}{ER + (Q_Y/Q_C)} \quad (5)$$

F_D and F_{DA} are the donor ECFP emission in the absence or presence of acceptor EYFP, respectively. Because F_D - F_{DA}/Q_C = SE/Q_Y, the net FRET (nF) = (F_D - F_{DA}) can be approximated as SE × Q_C/Q_Y. F_D, the fluorescence of the donor, is approximated as nF + F_{DA}. Q_Y and Q_C are the quantum efficiencies of EYFP and ECFP. Q_Y is 0.7 and Q_C is 0.4 (Griesbeck et al., 2001). The quantity SE/F_{DA} is measured as the corrected emission ratio (ER) described above.

Fluorescence microscopy and image processing

2 d after transfection, vin^{-/-}MECs were detached with trypsin and reseeded on a 20 μg/ml of fibronectin-coated delta T dish (Bioprotechs) equilibrated to 37°C. Images were captured at 37°C with a fluorescence microscope (model Axiovert 135TV; Carl Zeiss Microimaging, Inc.) equipped with a stage and objective heater (Bioprotechs), a Cool SNAP HQ camera (Photometrix), and Chroma filters. We used a 100× Plan Neofluor objective (Carl Zeiss Microimaging, Inc.) with an NA of 1.3 and collected the images with 2 × 2 binning. The excitation filter used for CFP was D436/10 nm. The emission filter used for CFP was D470/30 nm. The emission filter used for YFP was HQ535/30 nm. The beam splitter used was JP4 PC. FRET images were captured with the CFP excitation filter and YFP emission filter. Manipulations of numerical files were done using IPlab software (Scanalytics). Background images of CFP and FRET channels were captured from areas lacking cells on the experimental dish, using the same exposure times as for acquisition of the cell images.

The matched background images were subtracted from the fluorescent images to remove background and uneven illumination. After registration of the images, an empirically determined arithmetic averaging filter (blurring) was applied to the CFP and FRET images. This was done to minimize the presence of artificially high pixel ratios at the edges of focal adhesions. This artifact arises in part because the Airy disc of the FRET image is 11% larger than that of the CFP image. The pixel size on the CoolSnap HQ camera is 6.45 μm. In a 2 × 2 binned image, the diffraction limited spots at 100× for the objective are 3.9 pixels for YFP image and 3.4 pixels for the CFP image; these values are close to the width of the focal adhesions. Thus, a 3 × 3 or 5 × 5 pixel averaging filter was used to minimize the artifact generated by ratioing two different sized images (the FRET and the CFP image) of the same focal adhesions. Empirical selection of the filter was made by comparing the histograms of line segments drawn perpendicular to the long axis of the same focal adhesion region in both the CFP and FRET images. The averaging filters were adjusted such that the shapes of these histograms were as closely congruent as possible.

After the aforementioned manipulations, an image of the FRET ratio at each pixel (FR; Miyawaki and Tsien, 2000) was obtained by arithmetic manipulations of the CFP and FRET images according to the equation FR = I_{FRET}(probe)/I_{CFP}(probe). I_{FRET}(probe) and I_{CFP}(probe) denote the fluorescent intensity of FRET and CFP images at each pixel.

To determine the position of the cell edge, a threshold was selected empirically in the registered CFP image such that it included most of the cell boundary but excluded stray light at the cell edges. The segmentation and analysis tools in IPlab were used to estimate this threshold from the inflection point in the slope of a plot of pixel intensity versus pixel number along a line segment made perpendicular to the cell membrane. The sub-

threshold region will appear white in a pseudocolor ratio image, the same as background. The segmented CFP image was converted to a binary mask such that all pixels above the threshold were assigned a value of one and all those below were assigned a value of zero. The FRET ratio image was multiplied by the binary mask to remove pixels that had an artificially high ratio. The final ratio image was pseudocolored by assigning color values to the ratios. A linear scale from blue (low ratio and activated vinculin) to green/red (high ratio and closed vinculin) was constructed and a γ of 0.75 was applied to the display. The background and sub-threshold regions are color-coded white in the final FRET images.

To differentiate cytoplasm from focal adhesions for separate quantitation, two segmented images were generated, one for cytoplasm and one for adhesions. Image segmentation was performed in the registered CFP image. Each segmented image was converted to a binary image with the segmented region assigned a value of 1 and nonsegmented region assigned a value of zero. The FRET ratio image was then multiplied by each binary mask image to generate a FRET ratio image for focal adhesion or cytoplasm.

Permeabilized cell assay

Vin^{-/-} MECs were cultured on glass coverslips coated with PLL and 20 μ g/ml FN. After 16-h growth in 10% FCS/90% DME, the cells were washed briefly in assay buffer (5 mM MES, pH 6.1, 2 mM MgCl₂, 0.5 mM CaCl₂, 137 mM NaCl, 5.4 mM KCl, 4.2 mM NaHCO₃, and 0.1% glucose) and extracted for 1 min with ice-cold assay buffer plus 0.05% ultrapur digitonin (Calbiochem). After a 30-s rinse in ice-cold assay buffer, coverslips were incubated with the indicated proteins for 15 min at 4°C. Vinculin and Vh (residues 1–851) were used at a concentration of 25 μ g/ml and GST-vinexin (residues 1–329, encoding full length vinexin) at 10 μ g/ml in 25 mM MES, pH 6.0, 3 mM MgCl₂, and 1 mM EGTA. After two wash steps, cells were fixed in 4% PFA in PBS and stained with a monoclonal anti-vinculin and affinity-purified anti-GST antibodies. Oregon green donkey anti-mouse and RRX donkey anti-rabbit antibodies were used for immunofluorescence.

Online supplemental material

Fig. S1 shows immunoblots of cell lysates demonstrating integrity of FRET probes. Fig. S2 shows that an SDS-resistant structure in GFP causes aberrant migration in SDS-PAGE. Fig. S3 illustrates FRET in living cells as detected by the acceptor photobleach method. Fig. S4 demonstrates that vinculin is required for the recruitment of vinexin to focal adhesions in vinculin null cells. The protocol for cloning, expression, and purification of IpaA can be found in the online supplemental material. Online supplemental material is available at <http://www.jcb.org/cgi/content/full/jcb.200410100/DC1>.

We thank Dr. Douglas Murphy, Director of the Johns Hopkins University Microscope Facility, for help with setting up hardware and software for FRET imaging, Dr. Eileen Adamson for the vin^{-/-} cells, Dr. Jim Bear (University of North Carolina, Chapel Hill, NC) for advice on live cell imaging, Dr. David Shortle for use of the fluorimeter, and Drs. Chris Janetopoulos, Peter Devreotes, Mike Erickson, David Yue, Thomas Hofmann, and Hiro Okuno for helpful discussions on FRET.

This work was supported by an American Heart Association Postdoctoral Fellowship to H. Chen, Howard Hughes Medical Institute Predoctoral Fellowship to D. Cohen, and National Institutes of Health grant GM41605 to S. Craig.

Submitted: 19 October 2004

Accepted: 18 March 2005

References

Alenghat, F.J., B. Fabry, K.Y. Tsai, W.H. Goldmann, and D.E. Ingber. 2000. Analysis of cell mechanics in single vinculin-deficient cells using a magnetic tweezer. *Biochem. Biophys. Res. Commun.* 277:93–99.

Bakolitsa, C., J.M. de Pereda, C.R. Bagshaw, D.R. Critchley, and R.C. Liddington. 1999. Crystal structure of the vinculin tail suggests a pathway for activation. *Cell*. 99:603–613.

Bakolitsa, C., D.M. Cohen, L.A. Bankston, A.A. Bobkov, G.W. Cadwell, L. Jennings, D.R. Critchley, S.W. Craig, and R.C. Liddington. 2004. Structural basis for vinculin activation at sites of cell adhesion. *Nature*. 430: 583–586.

Balaban, N.Q., U.S. Schwarz, D. Riveline, P. Goichberg, G. Tzur, I. Sabanay, D. Mahalu, S. Safran, A. Bershadsky, L. Addadi, and B. Geiger. 2001. Force and focal adhesion assembly: a close relationship studied using

elastic micropatterned substrates. *Nat. Cell Biol.* 3:466–472.

Barstead, R.J., and R.H. Waterston. 1991. Vinculin is essential for muscle function in the nematode. *J. Cell Biol.* 114:715–724.

Bendori, R., D. Salomon, and B. Geiger. 1989. Identification of two distinct functional domains on vinculin involved in its association with focal contacts. *J. Cell Biol.* 108:2383–2393.

Beningo, K.A., M. Dembo, I. Kaverina, J.V. Small, and Y.L. Wang. 2001. Nascent focal adhesions are responsible for the generation of strong propulsive forces in migrating fibroblasts. *J. Cell Biol.* 153:881–888.

Borgon, R.A., C. Vornrhein, G. Bricogne, P.R. Bois, and T. Izard. 2004. Crystal structure of human vinculin. *Structure*. 12:1189–1197.

Bourdet-Sicard, R., M. Rudiger, B.M. Jockusch, P. Gounon, P.J. Sansonetti, and G.T. Nhieu. 1999. Binding of the *Shigella* protein IpaA to vinculin induces F-actin depolymerization. *EMBO J.* 18:5853–5862.

Byrne, B.J., Y.J. Kaczorowski, M.D. Coutu, and S.W. Craig. 1992. Chicken vinculin and meta-vinculin are derived from a single gene by alternative splicing of a 207-base pair exon unique to meta-vinculin. *J. Biol. Chem.* 267:12845–12850.

Chase, W., and F. Brown. 1997. General Statistics. 3rd ed. John Wiley & Sons, Inc., New York. 601 pp.

Clegg, R.M. 1992. Fluorescence resonance energy transfer and nucleic acids. *Methods Enzymol.* 211:353–388.

Coutu, M.D., and S.W. Craig. 1988. cDNA-derived sequence of chicken embryo vinculin. *Proc. Natl. Acad. Sci. USA.* 85:8535–8539.

Craig, S.W., and J.V. Pardo. 1983. Gamma actin, spectrin, and intermediate filament proteins colocalize with vinculin at costameres, myofibril-to-sarcolemma attachment sites. *Cell Motil.* 3:449–462.

Critchley, D.R. 2000. Focal adhesions—the cytoskeletal connection. *Curr. Opin. Cell Biol.* 12:133–139.

Danowski, B.A., K. Imanaka-Yoshida, J.M. Sanger, and J.W. Sanger. 1992. Costameres are sites of force transmission to the substratum in adult rat cardiomyocytes. *J. Cell Biol.* 118:1411–1420.

DeMali, K.A., C.A. Barlow, and K. Burridge. 2002. Recruitment of the Arp2/3 complex to vinculin: coupling membrane protrusion to matrix adhesion. *J. Cell Biol.* 159:881–891.

Erickson, M.G., B.A. Alseikhan, B.Z. Peterson, and D.T. Yue. 2001. Preassociation of calmodulin with voltage-gated Ca²⁺ channels revealed by FRET in single living cells. *Neuron*. 31:973–985.

Ervasti, J.M. 2003. Costameres: the Achilles' heel of Herculean muscle. *J. Biol. Chem.* 278:13591–13594.

Galbraith, C.G., K.M. Yamada, and M.P. Sheetz. 2002. The relationship between force and focal complex development. *J. Cell Biol.* 159:695–705.

Geiger, B. 1979. A 130K protein from chicken gizzard: its localization at the termini of microfilament bundles in cultured chicken cells. *Cell*. 18:193–205.

Goldmann, W.H., and D.E. Ingber. 2002. Intact vinculin protein is required for control of cell shape, cell mechanics, and rac-dependent lamellipodia formation. *Biochem. Biophys. Res. Commun.* 290:749–755.

Griesbeck, O., G.S. Baird, R.E. Campbell, D.A. Zacharias, and R.Y. Tsien. 2001. Reducing the environmental sensitivity of yellow fluorescent protein. Mechanism and applications. *J. Biol. Chem.* 276:29188–29194.

Horwitz, A., K. Duggan, C. Buck, M.C. Beckerle, and K. Burridge. 1986. Interaction of plasma membrane fibronectin receptor with talin—a transmembrane linkage. *Nature*. 320:531–533.

Huttelmaier, S., O. Mayboroda, B. Harbeck, T. Jarchau, B.M. Jockusch, and M. Rudiger. 1998. The interaction of the cell-contact proteins VASP and vinculin is regulated by phosphatidylinositol-4,5-bisphosphate. *Curr. Biol.* 8:479–488.

Huttelmaier, S., S. Illenberger, I. Grosheva, M. Rudiger, R.H. Singer, and B.M. Jockusch. 2001. Raver1, a dual compartment protein, is a ligand for PTB/hnRNPI and microfilament attachment proteins. *J. Cell Biol.* 155: 775–786.

Izard, T., G. Evans, R.A. Borgon, C.L. Rush, G. Bricogne, and P.R. Bois. 2004. Vinculin activation by talin through helical bundle conversion. *Nature*. 427:171–175.

Johnson, R.P., and S.W. Craig. 1994. An intramolecular association between the head and tail domains of vinculin modulates talin binding. *J. Biol. Chem.* 269:12611–12619.

Johnson, R.P., and S.W. Craig. 1995. F-actin binding site masked by the intramolecular association of vinculin head and tail domains. *Nature*. 373: 261–264.

Kioka, N., S. Sakata, T. Kawachi, T. Amachi, S.K. Akiyama, K. Okazaki, C. Yaen, K.M. Yamada, and S. Aota. 1999. Vinexin: a novel vinculin-binding protein with multiple SH3 domains enhances actin cytoskeletal organization. *J. Cell Biol.* 144:59–69.

Kotliansky, V.E., and G.N. Gneushev. 1983. Vinculin localization in cardiac

- muscle. *FEBS Lett.* 159:158–160.
- Kroemker, M., A.-H. Ruediger, B.M. Jockusch, and M. Ruediger. 1994. Intramolecular interactions in vinculin control α -actinin binding to the vinculin head. *FEBS Lett.* 355:259–262.
- Lee, S., and J.J. Otto. 1997. Vinculin and talin: kinetics of entry and exit from the cytoskeletal pool. *Cell Motil. Cytoskeleton.* 36:101–111.
- Maeda, M., E. Holder, B. Lowes, S. Valent, and R.D. Bies. 1997. Dilated cardiomyopathy associated with deficiency of the cytoskeletal protein metavinculin. *Circulation.* 95:17–20.
- Menkel, A.R., M. Kroemker, P. Bubeck, M. Ronsiek, G. Nikolai, and B.M. Jockusch. 1994. Characterization of an F-actin-binding domain in the cytoskeletal protein vinculin. *J. Cell Biol.* 126:1231–1240.
- Miyawaki, A., and R.Y. Tsien. 2000. Monitoring protein conformations and interactions by fluorescence resonance energy transfer between mutants of green fluorescent protein. *Methods Enzymol.* 327:472–500.
- Ohashi, T., D.P. Kiehart, and H.P. Erickson. 1999. Dynamics and elasticity of the fibronectin matrix in living cell culture visualized by fibronectin-green fluorescent protein. *Proc. Natl. Acad. Sci. USA.* 96:2153–2158.
- Olson, T.M., S. Illenberger, N.Y. Kishimoto, S. Huttelmaier, M.T. Keating, and B.M. Jockusch. 2002. Metavinculin mutations alter actin interaction in dilated cardiomyopathy. *Circulation.* 105:431–437.
- Ormo, M., A.B. Cubitt, K. Kallio, L.A. Gross, R.Y. Tsien, and S.J. Remington. 1996. Crystal structure of the *Aequorea victoria* green fluorescent protein. *Science.* 273:1392–1395.
- Otto, J.J. 1990. Vinculin. *Cell Motil. Cytoskeleton.* 16:1–6.
- Palecek, S.P., J.C. Loftus, M.H. Ginsberg, D.A. Lauffenburger, and A.F. Horwitz. 1997. Integrin-ligand binding properties govern cell migration speed through cell-substratum adhesiveness. *Nature.* 385:537–540.
- Pardee, J.D., and J.A. Spudich. 1982. Purification of muscle actin. *Methods Enzymol.* 85:164–181.
- Pardo, J.V., J.D. Siliciano, and S.W. Craig. 1983a. Vinculin is a component of an extensive network of myofibril-sarcolemma attachment regions in cardiac muscle fibers. *J. Cell Biol.* 97:1081–1088.
- Pardo, J.V., J.D. Siliciano, and S.W. Craig. 1983b. A vinculin-containing cortical lattice in skeletal muscle: transverse lattice elements (“costameres”) mark sites of attachment between myofibrils and sarcolemma. *Proc. Natl. Acad. Sci. USA.* 80:1008–1012.
- Patterson, G.H., and D.W. Piston. 2000. Forster distances between green fluorescent protein pairs. *Anal. Biochem.* 284:438–440.
- Pierobon-Bormioli, S. 1981. Transverse sarcomere filamentous systems: “Z and M cables.” *Journal of Muscle Research and Cell Motility.* 2:401–413.
- Price, G.J., P. Jones, M.D. Davison, B. Patel, A. Ben-Ze’ev, B. Geiger, and D.R. Critchley. 1989. Primary sequence and domain structure of chicken vinculin. *Biochem. J.* 259:453–461.
- Priddle, H., L. Hemmings, S. Monkley, A. Woods, B. Patel, D. Sutton, G.A. Dunn, D. Zicha, and D.R. Critchley. 1998. Disruption of the talin gene compromises focal adhesion assembly in undifferentiated but not differentiated embryonic stem cells. *J. Cell Biol.* 142:1121–1133.
- Rodriguez Fernandez, J.L., B. Geiger, D. Salomon, and A. Ben-Ze’ev. 1993. Suppression of vinculin expression by antisense transfection confers changes in cell morphology, motility, and anchorage-dependent growth of 3T3 cells. *J. Cell Biol.* 122:1285–1294.
- Shear, C.R., and R.J. Bloch. 1985. Vinculin in subsarcolemmal densities in chicken skeletal muscle: localization and relationship to intracellular and extracellular structures. *J. Cell Biol.* 101:240–256.
- Siliciano, J.D., and S.W. Craig. 1986. Isolation of meta-vinculin from chicken smooth muscle. *Methods Enzymol.* 134:78–85.
- Smith, D.B., and K.S. Johnson. 1988. Single-step purification of polypeptides expressed in *Escherichia coli* as fusions with glutathione S-transferase. *Gene.* 67:31–40.
- Street, S.F. 1983. Lateral transmission of tension in frog myofibers: a myofibrillar network and transverse cytoskeletal connections are possible transmitters. *J. Cell. Physiol.* 114:346–364.
- Subauste, M.C., O. Pertz, E.D. Adamson, C.E. Turner, S. Junger, and K.M. Hahn. 2004. Vinculin modulation of paxillin-FAK interactions regulates ERK to control survival and motility. *J. Cell Biol.* 165:371–381.
- Tan, J.L., J. Tien, D.M. Pirone, D.S. Gray, K. Bhadriraju, and C.S. Chen. 2003. Cells lying on a bed of microneedles: an approach to isolate mechanical force. *Proc. Natl. Acad. Sci. USA.* 100:1484–1489.
- Tigges, U., B. Koch, J. Wissing, B.M. Jockusch, and W.H. Ziegler. 2003. The F-actin cross-linking and focal adhesion protein filamin A is a ligand and in vivo substrate for protein kinase C α . *J. Biol. Chem.* 278:23561–23569.
- Xu, W., H. Baribault, and E.D. Adamson. 1998a. Vinculin knockout results in heart and brain defects during embryonic development. *Development.* 125:327–337.
- Xu, W., J.L. Coll, and E.D. Adamson. 1998b. Rescue of the mutant phenotype by reexpression of full-length vinculin in null F9 cells; effects on cell locomotion by domain deleted vinculin. *J. Cell Sci.* 111:1535–1544.
- Yang, F., L.G. Moss, and G.N.J. Phillips. 1996. The molecular structure of green fluorescent protein. *Nat. Biotechnol.* 14:1246–1251.
- Zamir, E., and B. Geiger. 2001. Molecular complexity and dynamics of cell-matrix adhesions. *J. Cell Sci.* 114:3583–3590.
- Zamir, E., B.Z. Katz, S. Aota, K.M. Yamada, B. Geiger, and Z. Kam. 1999. Molecular diversity of cell-matrix adhesions. *J. Cell Sci.* 112:1655–1669.
- Zemljic-Harpf, A.E., S. Ponrartana, R.T. Avalos, M.C. Jordan, K.P. Roos, N.D. Dalton, V.Q. Phan, E.D. Adamson, and R.S. Ross. 2004. Heterozygous inactivation of the vinculin gene predisposes to stress-induced cardiomyopathy. *Am. J. Pathol.* 165:1033–1044.